

Modeling the rotational and vibrational structure of the i.r. and optical spectrum of NH_3

STEPHEN L. COY* and KEVIN K. LEHMANN†

* Department of Chemistry 6-234B, Massachusetts Institute of Technology, 18 Vassar Street, Cambridge, MA 02139, U.S.A.; and † Department of Chemistry, Princeton University, Washington Road, Princeton, NJ 08544, U.S.A.

(Received 28 July 1988; in final form 7 September 1988; accepted 7 September 1988)

Abstract—Current progress on the rotational assignment of NH_3 vibrational bands from 4800 cm^{-1} to 18000 cm^{-1} is reported. We discuss a vibrational Hamiltonian for regions containing overtones or combinations of the three normal modes, excluding the symmetric inversion motion. The Hamiltonian is capable of modeling the normal mode to local mode transition observed in the spectrum as well as the observed band origins, rotational constants and intensities. It includes the Darling-Dennison (local mode-normal mode) coupling, the $(\nu_1, \nu_3)-2\nu_4$ Fermi resonance, and one significant $(\nu_1, \nu_3)-\nu_2$ interaction. We illustrate the intramolecular vibrational dynamics predicted by the model Hamiltonian.

INTRODUCTION

The vibrational spectrum of ammonia has been observed over the last half century by many workers, in many spectral regions [1]. Very early observations covered the full range from less than 1 cm^{-1} , into the optical region; that is, from the inversion tunneling motion of pyramidal NH_3 , to the red and green absorption bands which have been observed in reflection spectra of the outer planets. Using these observations to produce rotational and vibrational assignments of the dominant absorption regions for atmospheric diagnostics, and to refine our understanding of the structure, potential energy surface, and dynamics of NH_3 proved to be a difficult task. Today, most, but not all, of the bands expected through the N-H stretch fundamental region near 3400 cm^{-1} have been identified and rotationally analyzed. Some bands in that region have still not been located, and formulating a rotational Hamiltonian capable of reproducing the experimental data has often required the explicit inclusion of every nearby state. Above that region, only a few of the strongest, most isolated bands have been successfully studied.

The analysis of the NH_3 rovibrational spectrum is difficult because of the presence of multiple overlapping and strongly interacting bands in most of the spectral regions due to normal mode-local mode coupling and anharmonic resonances. The importance of carrying out these assignments lies in their use in several practical and theoretical research problems:

—Atmospheres of the outer planets contain large fractions of ammonia. Spectral assignments are necessary to determine atmospheric temperatures.
—As internal vibrational energy increases, the most accurate state description of the eigenstates is expected to change from the normal mode overtone and combination picture to a description in terms of local mode basis states. A vibrational Hamiltonian which can model this transition and which

includes other Fermi resonance couplings needs to be devised. The Hamiltonian can be tested by comparison of the experimental values with the predicted

- (i) Vibrational band origins.
- (ii) Vibrational band intensities.
- (iii) Rotational constants and Coriolis-coupling constants.

A potential energy function based on this Hamiltonian can be compared with *ab initio* calculations.

- A successful vibrational Hamiltonian provides a description of the intramolecular dynamics of ammonia. Spectroscopy can be translated into dynamics by asserting that a short pulse of light would create a pure local mode state which would then evolve as predicted by the Hamiltonian.
- Ammonia is one of the simplest hydrides, and is of fundamental theoretical and chemical interest. Its spectrum presents a continuing theoretical and experimental challenge to spectroscopists. The ammonia spectrum should be no less completely understood than the spectrum of water.

In this paper we are reporting current progress on a research program with two goals:

- (1) The rotational analysis of ammonia vibrational bands, beginning with the N-H stretch regions (including even quanta excitation of the asymmetric bend), then extending to regions with odd quanta in the asymmetric bend, and finally to symmetric bend regions.
- (2) Finding a vibrational Hamiltonian capable of predicting frequencies, intensities, and rotational structure of the bands, as well as their intramolecular dynamics.

Overcoming the difficulty of rotational assignment has been made possible by the development of the microwave detected microwave optical double res-

onance technique. Our theoretical work on the appropriate form of the vibrational Hamiltonian has resulted in a model capable of reproducing the observed band origins to within a few wavenumbers, and with considerable success in predicting constants and intensities. This paper includes analyses of vibrational bands and a discussion of an improved vibrational Hamiltonian not given in previous reports [2, 3].

EXPERIMENTAL

The microwave detected microwave optical double resonance apparatus is illustrated in Fig. 1. The effect of an intense pulse of i.r. or optical radiation is detected by monitoring the microwave absorption of a transition in the ground vibrational state of the sample. The use of a pulsed optical source allows the very high peak optical powers to transfer a significant population despite the weakness of vibrational overtone absorptions. The use of microwave detection means that non-fluorescing systems can be studied. When the optical radiation is in resonance with one of the two levels connected by the microwave field, a transient non-equilibrium population difference appears which undergoes transient mutation, as is described by the two-level Bloch equations. The microwave signal will be a damped oscillation with a frequency given by the microwave Rabi frequency, and damped by pressure-induced rotational energy transfer, and by the dephasing of M sublevels, each of which has a different Rabi frequency. A signal from the microwave (J, K) = (1, 1) Q branch in the ground vibrational state, which has a single detected M level, is shown in Fig. 2. The optical transition has been assigned as the $s^pP(1,1)$ transition at 9718.285 cm^{-1} . The optical radiation was generated by Stokes shifting in H_2 . Instead of being recorded in its entirety, as in Fig. 2, the signal is usually boxcar detected with a gate over the first peak. If the upper microwave connected level is depopulated by the optical field, the first peak of the transient mutation is absorptive; if the lower state, the first peak is emissive. The sign of the double resonance signal completely identifies the lower state, and its intensity is

Microwave Detected Microwave Optical Double Resonance

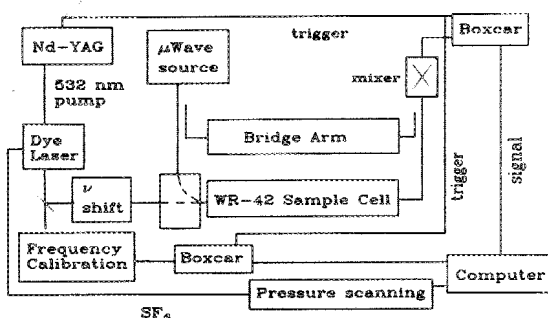


Fig. 1. Experimental apparatus for microwave-detected microwave optical double resonance. Phase-stabilized klystrons are used for the microwave source. A Nd:YAG pumped pulsed dye laser, with Raman shifting in H_2 for frequencies below $15\,000\text{ cm}^{-1}$, is the optical source. Boxcar detection measures the transient microwave response to optical depopulation of the ground state. Frequency calibration depends on the region, but may use I_2 absorption, the NH_3 photoacoustic absorption spectrum, or etalon fringes with known double resonance signals.

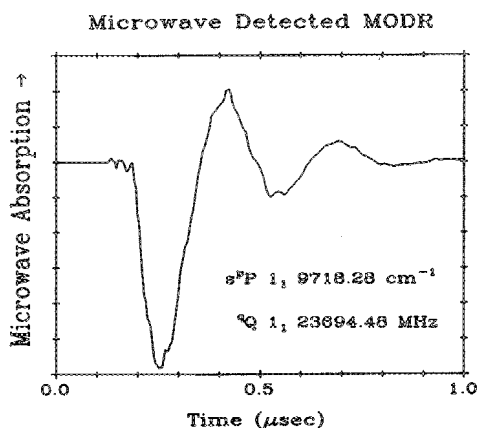


Fig. 2. A microwave transient nutation signal induced by an optical pulse. The ground state (J, K) = (1, 1) inversion double is monitored while the $s^pP(1,1)$ transition at 9718.285 cm^{-1} is pumped. Because the initial signal corresponds to less microwave absorption, the lower level of the microwave transition was depopulated.

proportional to the depopulation by the optical transition. The same technique may be applied to determine the frequency of upper state microwave transitions to high accuracy.

Progress on rotational analysis is made possible only by using as many different types of information as possible:

- High quality absorption spectrum taken at dry ice and room temperatures provide accurate line frequencies, and make it possible to estimate lower state energies from relative intensities.
- The basic double resonance data identifies the lower state of the transition and provides a reference transition for calculation of estimated lower state energies.
- The polarization dependence of double resonance can identify the optical transition as a P , Q or R branch for lower J values, or distinguish Q from P or R branches for higher J .
- The combination-difference technique of finding groups of lines terminating on a common upper level, can verify or suggest assignments. The predicted intensity and temperature dependence of lines in the group must also be consistent with the assignment.
- The line positions and intensities predicted from rotational fits to assigned lines must be used in cases where no double resonance data is available ($K=0$ states), and for upper states with no combination-differences. Many states are randomly perturbed by interactions with dark background states, so that predictions are useful only for very strong isolated lines.

ROTATIONAL ANALYSIS

Our work has focused on the regions containing N-H stretch overtones: $2\nu_{\text{NH}}$ through $6\nu_{\text{NH}}$. Of the four fundamental vibrations of NH_3 :

- ν_1 symmetric stretch at 3503 cm^{-1} ,
- ν_2 symmetric bend at 1030 cm^{-1} ,
- ν_3 asymmetric stretch at 3591 cm^{-1} ,
- ν_4 asymmetric bend at 1690 cm^{-1} ,

combinations of ν_1 , ν_3 and $2\nu_4$ appear in the N-H stretch regions and are coupled by Fermi resonance. This results in a total of 12 observable bands

being predicted in the $2\nu_{\text{NH}}$ region, which is shown in Fig. 3, and larger numbers for higher regions.

The current list of vibrational bands which we have analyzed from our double resonance data and absorption spectra is given in Table 1. Analysis of most of the regions below 15000 cm^{-1} are incomplete, and will be refined and published in detail at a later time. Band origins for the two bands near 6025 cm^{-1} , whose normal mode description is $(\nu_2 + \nu_3 + \nu_4)^2$, were given

previously by BENEDICT and PLYLER [4]. Line assignments for the bands at 4956 cm^{-1} and 5052 cm^{-1} , with which we generally agree, were given by SARANGI [5]. We have recently completed double resonance on the region near 8200 cm^{-1} , which may be described as $2\nu_{\text{NH}} + \nu_4$, and on the region near 9200 cm^{-1} , which is $2\nu_{\text{NH}} + \nu_4 + \nu_2$. Analysis on these bands is not yet complete enough to be reported. The listed bands have been analyzed using the symmetric top distort-

Table 1. Summary of bands analyzed

Sym.	cm^{-1}			$\text{cm}^{-1} \times 10^3$				Per cent of region
	Origin	B'	$C' - B'$	ζ'	D'_{JJ}	D'_{JK}	D'_{KK}	
$E(a)$	4956.787	10.149	-4.010	-0.245	3.2	9.0	-14.0	10
$E(s)$	4955.847	10.086	-3.962	-0.248	-3.0	18.0	-17.0	
$E(a)$	5052.97	9.991	-3.8172	-0.216	1.3	-2.9	2.1	85
$E(s)$	5052.60	9.965	-3.788	-0.212	0.4	-0.8	1.1	
$E(a)$	6037.12	9.786	-3.699	-0.225	-2.0	3.8	-1.8	
$E(s)$	6012.90	9.984	-3.928	-0.212	0.2	-0.4	0.5	
$A(a)$	6796.733	9.529	-3.260		-0.73	0.80	1.24	3
$A(s)$	6795.305	9.617	-3.359		0.74	-1.79	1.76	
$E(\text{ave})$	6566.22	10.266	-4.145	0.417				7
$E(a)$	6609.660	9.982	-3.853	0.041	2.7	-0.82	-3.44	50
$E(s)$	6608.833	9.999	-3.881	0.044	2.5	-1.99	-3.08	
E	~6666							10
$E(a)$	6677.951	9.955	-4.909	0.174	0.84	-28.9	-36.9	20
$E(s)$	6677.229	10.040	-4.895	0.147	2.36	-24.9	-34.5	
$E(a)$	6850.702	9.593	-3.372	-0.081	0.48	-0.41	-0.70	7
$E(s)$	6850.195	9.605	-3.363	-0.081	1.59	-3.02	1.67	
$E(a)$	9738.839	10.046	-4.089	0.041				10
$E(s)$	9738.152	10.085	-4.149	0.047				
$E(a)$	9689.722	10.098	-4.312	0.119				50
$E(s)$	9689.840	10.090	-4.308	0.122				
$E(a)$	9642.323	10.229	-4.396	-0.243				30
$E(s)$	9639.652	10.419	-4.609	-0.238				
E	~10066							
$E(s)$	10110.86	9.49	-3.12	-0.026				
$E(a)$	10111.31	9.58	-3.24	-0.023				
$A(s)$	10232.516	9.4365	-3.148		0.458	-1.723	1.467	1
$A(a)$	10234.734	9.491	-3.168					
$E(\text{ave})$	12628.2	9.75	-3.75	-0.02				40
$E(\text{ave})$	12675.5	11.0	-5.3	-0.13				30
$A(a)$	15447.38	9.12	-3.00					
$A(s)$	15450.82	9.16	-3.07					
$E(a)$	15448.70	9.14	-3.02	0.002				
$E(s)$	15451.19	9.22	-3.14	-0.006				
$A(a)$	18109.18	9.04	-3.11					
$A(s)$	18109.47	8.94	-2.90					
$E(a)$	18107.56	9.00	-2.84	~0				
$E(s)$	18109.47	8.94	-2.90					

Bands with no distortion constants listed were fit with ground state distortion constants.

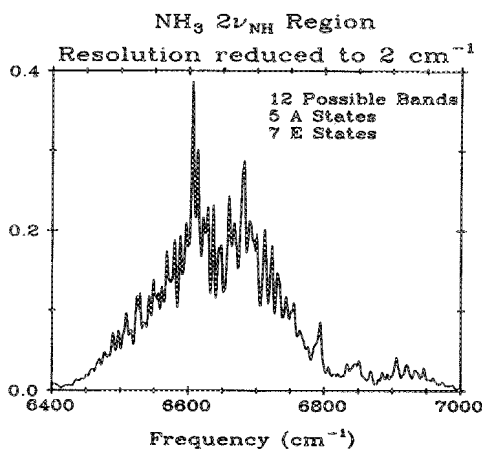


Fig. 3. A plot of the $2\nu_{\text{NH}}$ region at 200 K with the resolution artificially reduced to 2 cm^{-1} . The pressure-path was 7.2 mTorr. Twelve bands are predicted in this region (5 A states, 7 E states), and six have been assigned. The Q branch pile-up of the single assigned A state is visible near 6800 cm^{-1} .

able rotor Hamiltonian with coriolis coupling to express the upper state energies:

$$E'(J, K) = v_0 + B'J(J+1) + (C' - B')K^2 - 2C'\zeta kl - D'_{JJ}[J(J+1)]^2 - D'_{JK}J(J+1)K^2 - D'_{KK}K^4. \quad (1)$$

Lower state energies were taken from tabulated values [6]. In Table 1 where the distortion constants are not given, ground state distortion constants were used. Some of the upper bands are so perturbed that distortion constants are meaningless, while some of the lower bands will support higher order constants than those given.

VIBRATIONAL HAMILTONIAN

Our work has focused on the spectral regions where eigenstates should consist of mixtures of v_1 , v_3 and v_4 , excluding v_2 . The v_2 vibration is strongly anharmonic and thus more difficult to treat because of the double minimum potential in the inversion coordinate. Of the bands in Table 1, only the ones near 6050 cm^{-1} have considerable v_2 character, which is effectively measured by the inversion splitting, which is near 1 cm^{-1} , except for v_2 . A vibrational Hamiltonian containing the moderately anharmonic v_1 , v_3 and v_4 vibrations has been developed as the sum of the following contributions:

(1) A normal mode anharmonic expansion of the traditional form, but omitting v_2 terms:

$$\sum_{i=1,3,4} \omega'_i(n_i + d_i/2) + \sum_{i,j=1,3,4} x'_{ij}(n_i + d_i/2)(n_j + d_j/2) + \sum_{i,j=3,4} g'_{ij}l_i l_j. \quad (2)$$

This expression contains 11 adjustable parameters: three ω'_i values, six x'_{ij} values, and three g'_{ij} values. We add the prime to each adjustable constant to distin-

guish our fitted constants in our complete Hamiltonian from the values given in the traditional expansion with unrestricted sums, and with no other terms added to the Hamiltonian. The restriction of the sum, and the inclusion of other terms described below changes the meaning of some of these constants. The omission of v_2 from the sums means that the ω'_i values we determine contain the contribution of the omitted x_{i2} terms:

$$\omega_1 = \omega'_1 - \frac{x_{12}}{2} \quad (3.1)$$

$$\omega_3 = \omega'_3 - \frac{x_{32}}{2} \quad (3.2)$$

$$\omega_4 = \omega'_4 - \frac{x_{42}}{2}. \quad (3.3)$$

(2) The Darling-Dennison, or normal mode-local mode coupling terms which connect v_1 and v_3 [7]. These terms cause the transition to local mode states which dominate the transition intensity, and better describe the eigenstates as the internal energy increases. Because the bond with the greatest anharmonicity is the N-H bond, overtone transition intensity is expected to be concentrated in the N-H stretching vibrations. Because of that anharmonicity, the local mode model predicts that the lowest energy state, and the optically brightest, will put all excitation quanta in a single bond. Eigenstates are then approximately the one symmetric and two asymmetric combinations of this state which form A and E vibrations with degenerate band origins and similar rotational constants. This is observed in the $5\nu_{\text{NH}}$ and $6\nu_{\text{NH}}$ regions where the anharmonic resonance with v_4 , which may split the local mode states, is also tuned out of resonance. The matrix elements of this interaction involve two adjustable parameters, the effective resonance constants K_{1133} and K_{1333} :

$$(v_1 + 2, v_3 - 2, l_3 + 3, v_4, l_4 | H/hc | v_1, v_3, v_4, l_4) = \frac{K_{1133}}{4} \sqrt{(v_1 + 1)(v_1 + 2)(v_3 + l_3)(v_3 + l_3)} \quad (4.1)$$

$$(v_1 + 1, v_3 - 1, l_3 + 3, v_4, l_4 | H/hc | v_1, v_3, l_3, v_4, l_4) = \frac{3K_{1333}}{4} \sqrt{(v_1 + 1)(v_3 + l_3 + 2)(v_3 - l_3)(v_3 - l_3 - 2)} \quad (4.2)$$

$$(v_1 + 1, v_3 - 1, l_3 - 3, v_4, l_4 | H/hc | v_1, v_3, l_3, v_4, l_4) = \frac{3K_{1333}}{4} \sqrt{(v_1 + 1)(v_3 - l_3 + 2)(v_3 + l_3)(v_3 + l_3 - 2)} \quad (4.3)$$

These terms do not modify any of the terms in the anharmonic expansion in first order.

(3) The Fermi or anharmonic resonance between v_1 , or v_3 , and $2\nu_4$ greatly increases the complexity of each of the N-H stretch regions. Instead of including only states with constant $N = 2n_1 + 2n_3$, the block of

nearly isoenergetic states in each region contains all states of the same $N = 2n_1 + 2n_3 + n_4$. For simplicity, we consider only the lowest order interaction between these three modes. Because higher orders in perturbation theory introduce more matrix elements, this approximation may have to be removed as the model is refined. The cubic force constants K_{144} and K_{344} are the adjustable parameters in this interaction:

$$(v_1 - 1, v_3, l_3, v_4 + 2, l_4 | H/hc | v_1, v_3, l_3, v_4, l_4) \\ = \frac{K_{144}}{2\sqrt{2}} \sqrt{v_1(v_4 + l_4 + 2)(v_4 - l_4 + 2)} \quad (5.1)$$

$$(v_1, v_3 - 1, l_3 + 1, v_4 + 2, l_4 + 2 | H/hc | v_1, v_3, l_3, v_4, l_4) \\ = \frac{K_{344}}{4\sqrt{2}} \sqrt{(v_3 - l_3)(v_4 + l_4 + 2)(v_4 + l_4 + 4)} \quad (5.2)$$

$$(v_1, v_3 - 1, l_3 - 1, v_4 + 2, l_4 - 2 | H/hc | v_1, v_3, l_3, v_4, l_4) \\ = \frac{K_{344}}{4\sqrt{2}} \sqrt{(v_3 + l_3)(v_4 - l_4 + 2)(v_4 - l_4 + 4)} \quad (5.3)$$

These cubic force constants contribute to five of the parameters in the standard anharmonic expansion. Parameters that would be determined from the standard anharmonic expansion differ from our fitted (primed) constants by a contribution depending on the Fermi resonance cubic force constants. The two sets of parameters are related by

$$x_{14} = x'_{14} + 4\chi_1 \quad (6.1)$$

$$x_{34} = x'_{34} + 4\chi_3 \quad (6.2)$$

$$x_{44} = x'_{44} - \chi_1 - \chi_3 \quad (6.3)$$

$$g_{34} = g'_{34} + 4\chi_3 \quad (6.4)$$

$$g_{44} = g'_{44} + \chi_1 - \chi_3 \quad (6.5)$$

where

$$\chi_1 = \frac{K_{144}^2}{8(\omega_1 - 2\omega_4)} \quad (7.1)$$

$$\chi_3 = \frac{K_{344}^2}{8(\omega_3 - 2\omega_4)} \quad (7.2)$$

The x 's and g 's involving v_4 , given by these equations, are the only x or g values in our Hamiltonian for which the primed and unprimed terms differ.

The Hamiltonian thus described divides into blocks of the same $N = 2n_1 + 2n_3 + n_4$. Each of the constant N blocks divides into an A sub-block, with vibrational angular momentum $l = 0, 3, \dots$ and an E sub-block, with other l values. Of the A symmetry combinations, some have A_2 rather than A_1 symmetry, and are not accessible by dipole allowed transitions, although they may interact with A_1 states through A -axis coriolis. Since these states do not interact through any terms in our Hamiltonian with states of A_1 symmetry, and have no overlap with either the A_1 or the E local mode state, we make no attempt to remove them from each sub-block. For instance, in the $2v_{\text{NH}}$ region, the A

sub-block is of dimension 6, one state of which is of A_2 symmetry. The number of states in each sub-block grows rapidly with N , reaching 114 A states and 112 E states for $N = 12(6v_{\text{NH}}$ region).

(4) Sixteen free parameters are included in the three parts of the Hamiltonian described so far. MILLS and ROBIETTE [7] have used a single parameter description assuming all anharmonicity to be in the N-H bond to derive x - K relations which express six of the unknown parameters in terms of a Morse anharmonicity, x_{M} . These relations reduce the number of free parameters to 11:

$$x'_{11} = \frac{1}{3}x_{\text{M}} \quad (8.1)$$

$$x'_{13} = \frac{4}{3}x_{\text{M}} \quad (8.2)$$

$$x'_{33} = \frac{1}{2}x_{\text{M}} \quad (8.3)$$

$$g'_{33} = -\frac{1}{6}x_{\text{M}} \quad (8.4)$$

$$K'_{1133} = \frac{4}{3}x_{\text{M}} \quad (8.5)$$

$$K'_{3333} = \left(\frac{4}{9}\right)\sqrt{2}x_{\text{M}} \quad (8.6)$$

(5) Although we have neglected most contributions from v_2 states, such as the interaction $(v_1, v_3)3v_2^2$ which we believe is responsible for the large inversion splitting in the $4v_{\text{NH}}$ region and the inverted inversion order in the $5v_{\text{NH}}$ region [3], a distinct improvement in the quality of the fit has been achieved by including the largest second order contribution from the cubic force field to the x_{11} , x_{13} and x_{33} terms. By examining the empirical force field of HOY *et al.* [8], we found the K_{112} and K_{233} to be the most important, and have included them as adjustable parameters, bringing the total back to 13. The x - K relations alone give errors on the order of 20 per cent for the HOY *et al.* potential when compared with calculations from the full perturbation theory expressions [8,9]. That error drops to under 5 per cent when the new terms are added. These terms contribute to the first five x - K relations, so that the anharmonic constants are modified from the x - K relation values in Eqn. (8):

$$x_{11} = \frac{1}{3}x_{\text{M}} - \left(\frac{1}{4}\right)K_{112}^2 \frac{8\omega_1^2 - 3\omega_2^2}{\omega_2(4\omega_1^2 - \omega_2^2)} \quad (9.1)$$

$$x_{33} = \frac{1}{2}x_{\text{M}} - \left(\frac{1}{4}\right)K_{233}^2 \frac{8\omega_3^2 - 3\omega_2^2}{\omega_2(4\omega_3^2 - \omega_2^2)} \quad (9.2)$$

$$x_{13} = \frac{4}{3}x_{\text{M}} - \frac{K_{113}K_{233}}{\omega_2} \quad (9.3)$$

$$g_{33} = -\frac{1}{6}x_{\text{M}} - \left(\frac{1}{4}\right)K_{233}^2 \frac{\omega_2}{4\omega_3^2 - \omega_2^2} \quad (9.4)$$

$$K_{1133} = \frac{4}{3}x_M + K_{112}K_{233} \frac{\omega_2}{4\omega_{13}^2 - \omega_2^2} \quad (9.5)$$

where

$$\omega_{13} = (\omega_1 + \omega_3)/2.$$

Since the x - K relations express six parameters in terms of the single anharmonicity, x_M , but we have reintroduced K_{112} and K_{233} as fitted parameters, the model has a total of 13 free parameters.

MODEL OPTIMIZATION

Input to the fit consists of the band origins of all observed vibrational bands with no ν_2 contribution, as shown in Table 1. These states are identified by inversion splittings close to the ground state value of 0.7 cm^{-1} . Rotational constants shown in this table are subject to refinement as analysis of many of the bands is incomplete. The results of the fit are shown in Table 2, which gives the input and calculated band origins. Some bands of Table 1 are omitted from Table 2 because their assignments, either rotational, or to eigenstates in the fit, are uncertain. Table 3 gives the model parameters and a comparison with values from the HOY *et al.* valence force field and the fourth order Moller-Plesset calculation of HARGISS and ERMLER [13]. The HARGISS and ERMLER calculation predicts smaller cubic force constants than the valence force

field. Our fitted value of K_{233} is well determined, and lies between the two predictions. We express their results in terms of our fitted constants because the presence of near resonant denominators in the corrections makes the traditional parameters very sensitive to the tuning of the Fermi resonance. The values in the table are more stable to small changes in the fit or in the calculation. Other calculations have been reported, but insufficient information was given to compare with our fitted constants [14, 15].

The r.m.s. error in the fitted origins is 3.3 cm^{-1} . When the full model containing 16 free parameters is fitted to the data, the r.m.s. deviation drops to 2.2 cm^{-1} , but the calculated errors in the model parameters are increased because of correlations between the parameters. Some of the parameters were also changed more than the 13-parameter uncertainty, but still within the overlapping uncertainties of the two fits. Because the x - K relations correctly represent the majority of the variation of the six connected parameters, especially with the addition of the two cubic terms, we feel that the data doesn't support determination of the 16 parameters independently. The cubic force field is also related to the ground state sextic distortion constants (H constants), and to the change in rotational constant with vibrational excitation (α constants) [16]. In the future, we will try to determine the cubic force constants from these other sources. The uncertainties in the fit are also increased by the

Table 2. $n_2=0$ states of NH_3 . Band origins of states without ν_2 character compared to the vibrational Hamiltonian predictions. The normal mode assignments are approximate, based on the eigenfunctions

(n_1, n_3, n_4)	$E(\text{cm}^{-1})$ obs. (s symmetry)	Ref.	$E(\text{cm}^{-1})$ calc.
(0, 0, 1 ¹)	1626.1	[4]	1627.2
(0, 0, 2 ⁰)	3216.1	[4]	3218.2
(1, 0, 0)	3336.1	[10]	3337.2
(0, 0, 2 ²)	3240.0	[4]	3239.1
(0, 1 ¹ , 0)	3443.6	[10]	3440.9
(1, 0, 1 ¹)	4955.9	This work	4955.8
(0, 1 ¹ , 1 ¹)	5052.6	This work	5052.3
(1, 0, 2 ⁰)	(6520)	[11]	6520.3
(2, 0, 0)	6606.0	[11]	6601.6
(0, 2 ⁰ , 0)	6793.0	This work	6797.1
(1, 0, 2 ²)	6556.0	This work	6555.2
(1, 1 ¹ , 0)	6608.0	[4], This work	6605.9
(0, 1 ¹ , 2 ⁻²)	6676.0	This work	6680.1
(0, 2 ² , 0)	6850.0	[4], This work	6846.7
(2, 0, 1 ¹)	(8200)	[12]	8197.3
(1, 0, 4 ²)	9641.0	This work	9643.6
(2, 1 ¹ , 0)	9690.0	This work	9683.9
(0, 1 ¹ , 4 ⁰)	9739.0	This work	9740.3
(0, 0, 3 ¹)	10111.0	This work	10114.3
(0, 0, 3 ³)	10232.0	This work	10233.2
(1, 0, 6 ²)	12628.0	This work	12636.8
(3, 1 ¹ , 0)	12676.0	This work	12672.6
(5, 0, 0)	15450.8	This work	15449.3
(4, 1 ¹ , 0)	15451.2	This work	15449.7
(6, 0, 0)*	18107.5	This work	18095.6
(5, 1 ¹ , 0)*	18109.0	This work	18095.6

*Levels not used in fit.

Table 3. Model parameters for the vibrational Hamiltonian. Empirical force field results from Ref. [8]. *Ab initio* results from Ref. [13]

Best fit				
Parameter	cm ⁻¹	(1σ)	Empirical	<i>Ab initio</i>
ω'_1	3484.59	(11.2)	3498.6	3537.6
ω'_3	3623.72	(11.9)	3583.1	3677.9
ω'_4	1677.83	(5.9)	1672.1	1736.7
x'_{14}	-14.64	(4.6)	-35.88	-23.66
x'_{34}	-19.51	(4.5)	-33.29	-25.04
x_{44}	-8.89	(1.1)	-8.11	-4.37
x'_{34}	3.94	(6.6)	4.98	6.07
x_{44}	3.10	(2.2)	1.11	2.62
K_{144}	50.05	(5.8)	121.9	78.33
K_{344}	-36.83	(8.3)	-70.8	-65.73
K_{112}	-48.7	(94.0)	119.5	73.97
K_{233}	122.0	(19.0)	165.4	61.42
x_M	-74.05	(2.0)		
Predicts				
x_{11}	-25.83		-29.81	-28.61
x_{13}	-92.96		-114.96	-107.04
x_{33}	-44.18		-52.25	-48.36
θ_{33}	12.26		14.50	15.36
K_{1133}	-98.86			
K_{1333}	-46.59			

missing data for bands which are weak in one photon absorption in each region. The resonance Raman data of ZIEGLER [11] has been helpful because it gives information on *A* states, although at low resolution. Additional data on states with ν_4 excited is also necessary. We also expect to be able to identify more bands from the absorption spectrum and double resonance, especially in the $3\nu_{\text{NH}}$ and $4\nu_{\text{NH}}$ regions, and in the $2\nu_{\text{NH}} + \nu_4$ and $3\nu_{\text{NH}} + \nu_4$ regions.

We have seen both from the spectrum, and from the eigenvectors of the model Hamiltonian, that the Fermi resonance (ν_1, ν_3)- $2\nu_4$ finally tunes out of resonance at the $5\nu_{\text{NH}}$ level. The local mode states are no

longer split by that interaction, and appear as essentially degenerate *A* and *E* states. In order to look for the onset of local mode character, we have predicted the eigenstates with the Fermi resonance turned off. Then the $2\nu_{\text{NH}}$ region still shows normal mode states, but in $3\nu_{\text{NH}}$, the states have local mode character. The complexity of the $3\nu_{\text{NH}}$ and $4\nu_{\text{NH}}$ regions then comes from the ν_4 anharmonic resonance.

We have used the experimental values for the normal mode fundamental coriolis coupling constants and rotational constants to predict the spectroscopic constants of bands in each region. The values were estimated by linearly combining the changes in rota-

Table 4. Comparison of observed rotational and coriolis coupling constants with calculated values. Predictions were calculated from vibrational eigenvectors and spectral constants of fundamentals. All values in cm⁻¹. See text for discussion

Energy (obs.)	<i>B</i> (obs.)	<i>B</i> (calc.)	ζl (obs.)	ζl (cals.)
6795.3	9.62	9.63		
6556.2	10.27	10.27	0.417	0.481
6608.8	10.00	9.97	0.044	0.027
6677.2	10.04	9.92	0.147	-0.012
6850.2	9.61	9.62	-0.081	-0.078
9639.7	10.42	10.47	-0.238	0.438
9689.8	10.09	10.18	0.122	-0.066
9738.2	10.08	9.99	0.047	-0.044
10110.9	9.49	9.52	-0.026	-0.014
10232.5	9.44	9.45		
12628.2	9.75	9.84	-0.02	0.105
12675.5	11.0	10.55	-0.13	0.332
15450.8	9.16	9.14		
15451.2	9.22	9.13	-0.006	0.001
18109.47	8.94	8.92	~0	-0.0007

Table 5. Observed and calculated band intensities for perpendicular bands in the $2\nu_{\text{NH}}$ and $3\nu_{\text{NH}}$ regions

Predicted frequency (cm ⁻¹)	Observed frequency (cm ⁻¹)	Calculated intensity	Observed intensity
$2\nu_{\text{NH}}$			
6374.4		0.0009	
6429.3		0.0001	
6554.7	6566.2	0.0134	0.07
6607.3	6609.3	0.3869	0.50
6642.9	6666.0	0.0114	0.10
6677.9	6677.5	0.5436	0.20
6848.8	6850.4	0.0437	0.07
$3\nu_{\text{NH}}$			
9645.9	9640.9	0.025	0.10
9689.3	9689.8	0.317	0.50
9742.1	9738.5	0.535	0.30

tional constants between the ground state and the vibrational fundamentals according to the model eigenstate decomposition. Table 4 shows some selected results for B and ζl (values of $C-B$ are omitted because C varies little between the bands). The rotational constants agree quite well, but the coriolis constants have some glaring disagreements. The reason for the disagreements is hoped to be neglected interactions between bands, especially since the bands listed in Table 4 are ones for which no predicted bands with the needed coriolis constants are nearby.

The intensity predictions of our model are based on overlap with either the A or the E local mode state of the region. This predicts intensities among the A states, or among the E states, but not the A/E ratio. In the $2\nu_{\text{NH}}$ region, we have observed five E states and in the $3\nu_{\text{NH}}$ region, four E states. Their observed intensities are compared with predicted values in Table 5. The strongest bands are correctly identified, but the weaker bands are predicted to be weaker than observed. The extra intensity may come from other motions than the pure N-H stretch.

INTRAMOLECULAR DYNAMICS

Translation of a successful model Hamiltonian into a dynamical model with sub-picosecond resolution and its predictions can be understood from several assertions which are based on physical principles, on assumptions about the source of optical intensity, and on the dynamical character and accuracy of the model:

—We assume that the overtone intensity is dominated by the most anharmonic motion, the N-H stretch. This means that local mode states carry all the transition intensity, and that projections of the eigenstates onto the local mode states give the relative intensities within each A or E block. A short pulse of light will prepare the non-stationary bright state, the local mode state.

—An initially prepared state will evolve according to the model Hamiltonian. We will find two types of predictions:

- (i) The local mode state in a Fermi resonance region will rapidly delocalize into states with multiple quanta of ν_4 excited.
- (ii) The local mode state in the higher regions with the Fermi resonance detuned, and with essentially local mode character, will retain a large overlap with the initial state.

—The Fourier transform relationship between spectrum and dynamics indicates that an accuracy of about 3 cm^{-1} will allow the autocorrelation function of the local mode state to be followed correctly for about 2 ps. Overlap integrals with other states depend on expansion coefficients of the eigenstates, and may have larger errors than the autocorrelation, but still should be qualitatively correct for about the same period of time.

The dynamics can be measured by the time-dependence of overlap integrals with the state propagated from the initial local mode state. We can examine either the time resolved expression, or the time averaged value:

$$P_{ab}(t) = |\langle \Psi_b(t) | \Psi_a(0) \rangle|^2 \quad (10)$$

or

$$\bar{P}_{ab} = \lim_{T \rightarrow \infty} \frac{1}{T} \int_0^T P_{ab}(t) dt \quad (11)$$

Where the state a is the initial local mode state, $P_{aa}(t)$ gives the survival probability of the initial local mode state. The quantity $P_{ab}(t)$ measures the transfer from state a (the local mode state) to state b (some other state in the region) with time. If we use the unperturbed basis for state b , and sum over all states b in one N-H stretch region with a given number of ν_4 quanta excited, we observe the rate at which the Fermi resonance brings that number of ν_4 quanta into the dynamics.

Table 6. Time-averaged survival probability of initially prepared local mode states in each N-H stretch overtone region. Until the 5 ν_{NH} region, local mode states are delocalized by Darling-Dennison and/or anharmonic resonance with ν_4

n_{NH}	\bar{P}_{aa}	
	A symmetry	E symmetry
1	0.820	0.967
2	0.347	0.396
3	0.263	0.334
4	0.331	0.334
5	0.807	0.815
6	0.902	

Table 6 lists the time averaged survival probability of the initial local mode state. We see that initial state retains its local mode character for the 5 ν_{NH} and 6 ν_{NH} regions. HELLER [17] has noted that $(\bar{P}_{aa})^{-1}$ gives the effective number of states that the dynamics populates. Table 7 gives the time averaged values of the overlap of the initial local mode states with all states in the same region with each possible number of ν_4 quanta excited. These values show the effectiveness of the Fermi resonance interaction in bringing the overtones of the ν_4 vibration into the molecular dynamics.

Time dependent behavior is shown in Figs 4-6. Figure 4 shows the rapid decay of the 3 ν_{NH} local mode state. The dynamics of the local mode state may involve the normal mode stretches or the ν_4 states accessed by the Fermi resonance. Because the 3 ν_{NH} region is strongly mixed by Fermi resonance with 2 ν_4 , the overlap with even quanta of ν_4 is expected to increase rapidly and hold a significant average value. Figure 5 shows the 3 ν_{NH} local mode state $P_{ab}(t)$, summed over basis states with 4 ν_4 excited. Figure 6 gives the autocorrelation function of the 5 ν_{NH} state, which is a local mode region, with the Fermi resonance detuned, and shows a sustained overlap with the initial state.

Table 7. Time average overlap between N quanta local mode state and all states with M quanta of ν_4 excited

N_{NH}	$\Sigma \bar{P}_{ab}$							
	$M=0$	2	4	6	8	10	12	
A symmetry								
1	0.820	0.180						
2	0.621	0.338	0.004					
3	0.379	0.241	0.341	0.004				
4	0.367	0.131	0.210	0.204	0.008			
5	0.832	0.078	0.026	0.025	0.023	0.014		
6	0.918	0.444	0.011	0.007	0.008	0.006	0.005	
E symmetry								
1	0.967	0.033						
2	0.463	0.508	0.028					
3	0.378	0.212	0.359	0.048				
4	0.359	0.155	0.221	0.174	0.090			
5	0.837	0.080	0.028	0.024	0.017	0.012		

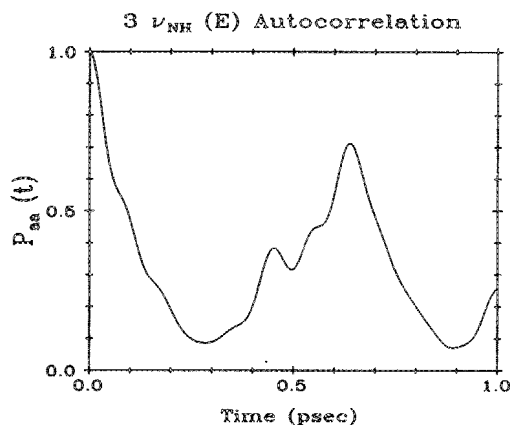


Fig. 4. $P_{aa}(t)$ for the 3 ν_{NH} region gives the survival probability of an initial local mode state. The local mode state is not an approximate eigenstate in this region, so overlap with the local mode state is rapidly lost.

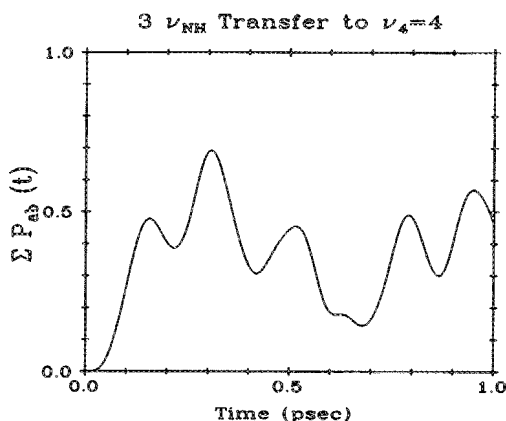


Fig. 5. $P_{ab}(t)$ for the 3 ν_{NH} region with state $b=4\nu_4$ shows the transmission of the local mode excitation through the Fermi resonance into ν_4 .

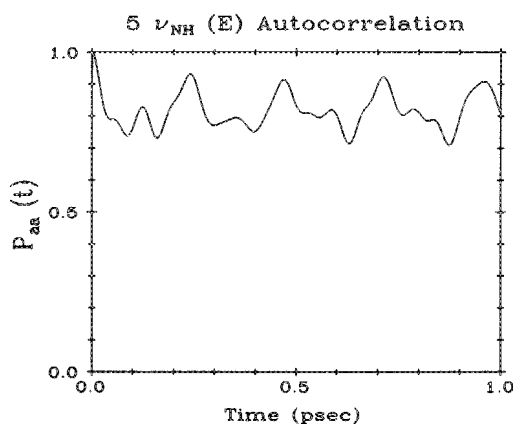


Fig. 6. $P_{aa}(t)$ for the $5\nu_{\text{NH}}$ region indicates that the local mode state is an approximate eigenstate. The local mode state survival probability drops somewhat initially, but maintains a high average value.

CONCLUSION

Microwave-detected microwave optical double resonance has made possible the rotational analysis of many NH_3 overtone and combination vibrational bands. This has allowed the development of an approximate vibrational Hamiltonian which has been reasonably successful in predicting band origins, rotational constants, and intensities of the bands. The analysis could be improved by using other data (ground state centrifugal distortion constants, and ΔB for the fundamentals) to obtain the cubic force field, and by devising some method of exciting and assigning the weaker bands in each region.

Acknowledgements—We appreciate the use of the facilities of the M.I.T. Laser Research Center, a National Science Foundation regional instrumentation facility for the double resonance experiments. Dr DON RAMSAY and BILL NEIL of the Herzberg Institute of the Canadian National Research Council made available to us, and assisted us in the use of, their BOMEM Fourier transform spectrometer and long path White cells which we used to obtain absorption spectra

of ammonia from 4800cm^{-1} to 12800cm^{-1} . Professors WALTER ERMILER and LAWRENCE ZIEGLER provided results in advance of publication. Professors IAN MILLS, MARTIN QUACK, ROBERT FIELD, WILLIAM KLEMPERER and E. BRIGHT WILSON, have added their insights in discussing this work with us. This work was supported by the National Science Foundation through a Presidential Young Investigator award to K. K. LEHMANN, and by the Donors of the Petroleum Research Fund, administered by the American Chemical Society.

REFERENCES

- [1] Early work on ammonia is reviewed in G. HERZBERG, *Infrared and Raman Spectra*. Van Nostrand Reinhold, Princeton (1945). Early references are also listed in Ref. [1] of Ref. [2] of this paper.
- [2] K. K. LEHMANN and S. L. COY, *J. chem. Soc. Faraday Trans. II* **84**, 000 (1988).
- [3] S. L. COY and K. K. LEHMANN, *J. chem. Phys.* **84**, 5239 (1986). The formula given for $(n_1-1, n_2+3 | H/hc | n_1, n_2)$ is in error. An errata is being published.
- [4] W. S. BENEDICT and E. K. PLYLER, *Can. J. Phys.* **35**, 1235 (1957).
- [5] J. SARANGI, *J. Quant. Spectrosc. Rad. Transf.* **18**, 257 (1957).
- [6] S. URBAN, D. PAPOUSEK, J. KAUPPINEN, K. YAMADA and G. WINNEWISER, *J. molec. Spectrosc.* **101**, 1 (1983).
- [7] I. M. MILLS and A. G. ROBIETTE, *Adv. chem. Phys.* **57**, 1 (1984).
- [8] A. R. HOY, I. M. MILLS and G. STREY, *Molec. Phys.* **24**, 1265 (1973).
- [9] I. M. MILLS in *Molecular Spectroscopy: Modern Research* (edited by K. NARAHARI RAO and C. W. MATHEWS). Academic Press, New York (1972).
- [10] R. ANGSTL, H. FINSTERHOLZL, H. FRUNDER, D. ILLIG, D. PAPOUSEK, P. PRACNA, K. N. RAO, H. W. SCHROTTER and S. URBAN, *J. molec. Spectrosc.* **101**, 1 (1983).
- [11] LAWRENCE ZIEGLER, private communication.
- [12] H. SASADA, *Opt. Lett.* **9**, 448 (1984).
- [13] L. O. HARGISS and W. C. ERMILER, *J. phys. Chem.*, to be published.
- [14] J. F. GAW and N. C. HANDY, *Chem. Phys. Lett.* **121**, 321 (1985).
- [15] P. PULAY, J.-G. LEE and J. E. BOGGS, *J. chem. Phys.* **79**, 3382 (1983).
- [16] M. R. ALIEV and J. K. G. WATSON, *J. molec. Spectrosc.* **61**, 29 (1976).
- [17] E. J. HELLER, *Faraday Discuss. chem. Soc.* **75**, 141 (1983), and references therein.